Faraday Discussions

Cite this: Faraday Discuss., 2022, 235, 416



PAPER

View Article Online View Journal | View Issue

Superlattice ordering transitions driven by short-range structure in barium calcium carbonates

Michael. L. Whittaker, D†** Efrat Pri-gal, Asher Schmidt b and Derk Joester 🕩 a

Received 9th November 2021, Accepted 2nd February 2022

DOI: 10.1039/d1fd00086a

Balcite $(Ba_xCa_{1-x}CO_3)$ is a synthetic analog of rhombohedral carbonate minerals like calcite and dolomite that is disordered on both the cation and anion sublattices. Here, we show that multiple exotic superlattice structures, including a dolomite analog that we call balcomite, can form from balcite at elevated temperatures. The second-order balcite-to-balcomite conversion at temperatures between 150-600 °C is driven by the preference of barium and calcium for different oxygen coordination numbers and facilitated by local carbonate reorientation. At elevated pressure, further superlattice order arises from cation segregation in all three dimensions, producing a supercell with the same $R\bar{s}m$ symmetry as balcite but 6 imes larger. This highly ordered structure relaxes back to the balcomite structure upon returning to ambient conditions. None of the three naturally occurring polymorphs of Ba_{0.5}Ca_{0.5}CO₃ (alstonite, paralstonite, barytocalcite) formed from balcite despite being putatively energetically favored. Instead, alstonite transformed to a balcomite-like structure via a first-order process after transiently converting to a paralstonite-like structure via a second-order process. Together, these results show that high temperature transformation pathways between structures in the barium calcium carbonate system can be driven by coarsening and are facilitated by similarity in short-range order, conceptually analogous to previously described low-temperature transformations. Many of the exotic high temperature carbonate structures are unstable, but may participate in transformation pathways between naturally observed metastable mineral phases, suggesting important roles for ephemeral phases in shaping past and current mineral distributions.

^aDepartment of Materials Science and Engineering, Northwestern University, 2220 Campus Dr. Evanston, IL, 60208, USA. E-mail: mwhittaker@lbl.gov

^bSchulich Faculty of Chemistry and Russell Berrie Nanotechnology Institute, Technion – Israel Institute of Technology, Haifa 32000, Israel

[†] Current address: Energy Geosciences Division, Lawrence Berkeley National Laboratory, 1 Cyclotron Rd, Berkeley, 94720, CA, USA.

Introduction

Mixed-cation CaCO₃–BaCO₃ phases play a unique biogeochemical role as alkaline carbonate sediments,^{1,2} paleoclimate proxies,³⁻⁵ and biologically induced precipitates^{6,7} including the first known cyanobacterial intracellular biominerals.^{8,9} All natural and experimentally synthesized structures in this system lie within the metastability window¹⁰ approximately 20 kJ mol⁻¹ above ground-state, phase-separated calcite (CaCO₃) and witherite (BaCO₃), and below amorphous calcium barium carbonate (ACBC, Ba_xCa_{1-x}CO₃).^{11,12} However, simulations indicate that only a few of many possible structures occur naturally in the lithosphere despite relatively small energy differences between myriad metastable phases.¹³ If differences in stability are small relative to the barriers to interconversion between phases, as they appear to be in the CaCO₃–BaCO₃ system,¹⁴ a better understanding of mineral transformation pathways may offer important insight into how these minerals are distributed and their implications for reconstructing past conditions.¹⁵

Despite its persistence for months in aqueous solution, ¹² balcite (Ba_{0.5}Ca_{0.5}CO₃ with $R\bar{3}m$ symmetry) is unstable relative to calcite and witherite^{11,12} and, putatively, to three naturally occurring Ba_{0.5}Ca_{0.5}CO₃ polymorphs (alstonite, paralstonite, barytocalcite).^{2,16,17} Both the carbonate anion orientation and cation distribution are highly disordered in balcite, ^{18,19} while the naturally occurring polymorphs are thought to have both cation and carbonate order.^{17,20} Here, we investigate the recrystallization of Ba_{0.5}Ca_{0.5}CO₃ polymorphs at elevated temperatures and find evidence for complex crystallization pathways among many exotic carbonate structures. Importantly, we show that long-range ordered structures form through continuous, second-order transformation from precursors with similar short-range order, but that interconversion between structures with distinct short-range order occurs *via* discontinuous, first-order transitions.

Results

hr-pXRD, Rietveld refinement, and in situ MAXS/WAXS

Balcite was synthesized under ambient conditions and subsequently annealed at a controlled rate in order to observe the products and pathways by which it transforms. As-synthesized balcite with x = 0.50 (Fig. 1a) was annealed to 600 °C

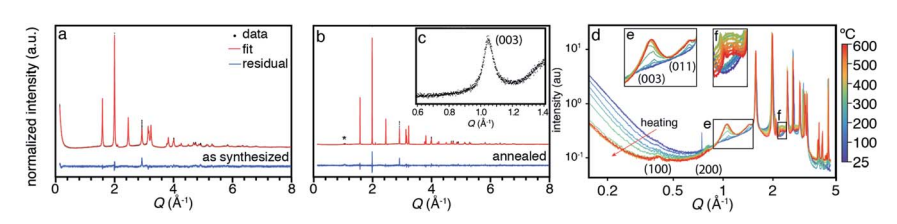


Fig. 1 (a) hr-pXRD of as-synthesized balcite and (b) balcite annealed to 600 °C. (c) A small, broad peak emerged at $Q=1.05\,\text{Å}^{-1}$, consistent with a superlattice reflection along the c-axis. (d) In situ WAXS/MAXS of balcite during heating from 25–600 °C. (e) Gradual emergence of superlattice reflections. (f) Abrupt formation of peaks associated with carbonate ordering.

(Fig. 1b and c) at a rate of 10 °C minute⁻¹ and held for 10 minutes, which led to a significant decrease in the width of Bragg peaks that were initially very broad. As-synthesized balcite had an average grain size of 34 ± 4 nm, consistent with previous measurements, while annealed balcite grains exceeded 250 nm, as determined by Rietveld refinement. Loss of diffraction intensity at scattering vectors $Q < 0.5 \text{ Å}^{-1}$ in the annealed sample is consistent with a reduction in smallangle scattering from nanoscale grains (Fig. 1b and c). Scattering intensity at $Q < 0.5 \text{ Å}^{-1}$ in as-synthesized balcite shifted to lower Q in medium- and wide-angle X-ray scattering (MAXS/WAXS) collected simultaneously while heating *in situ*, and diffraction peaks also grew narrower as the temperature increased (Fig. 1d–f). Together, these observations indicate that initially nanoscale grains coarsened at elevated temperature. Coarsening began around 150 °C, with grains appearing to reach a constant size by 500 °C, at which point the peak widths and small-angle scattering intensity did not change appreciably.

Coarsened grains also adopted crystalline order that was distinct from the assynthesized nanocrystalline material. Most notably, a peak at $Q=1.05~\text{Å}^{-1}$ emerges around 150 °C and grows until around 500 °C, concurrent with coarsening. The gradual appearance of this reflection during *in situ* heating is indicative of compositional evolution on alternating cation lattice planes, and is consistent with the self-segregation of barium and calcium that were initially randomly mixed. This peak is analogous to the (003) superlattice ordering peak observed in dolomite^{21,22} that is associated with the segregation of Ca and Mg to alternating lattice planes, doubling the unit cell along the c axis. Cation superlattice order that is consistent with $R\bar{3}c$ symmetry in a unit cell with $c=2c_{\text{balcite}}$ persisted after the sample was cooled, an indication of quenched crystallographic reorganization that was irreversible at ambient conditions.

Additional peaks at Q=0.405 Å⁻¹, 0.810 Å⁻¹, 1.43 Å⁻¹, and 2.20 Å⁻¹ emerged over this temperature range during *in situ* heating (Fig. 1d), which occurred within a hermetically sealed aluminum crucible, but were not observed after the sample was returned to ambient temperature and pressure (Fig. 1b and c). This suggests that additional structural evolution occurs at elevated pressure inside the sealed crucible, which is likely due to trapped structural water in the as-synthesized material (see section on NMR). These peaks are consistent with a superlattice structure that forms along both the a and c axes. In addition to the superlattice peak at Q=1.05 Å⁻¹, peaks Q=0.405 Å⁻¹ and 0.810 Å⁻¹ correspond to (100) and (200) reflections from a cell with $a=3a_{\rm balcite}\cong 17.95$ Å, and the peak at Q=1.433 Å⁻¹ is a superlattice reflection of the balcite (022) at Q=2.866 Å⁻¹ (Fig. 1e). Thus, under pressure the system evolves towards an $R\bar{3}m$ supercell with $a/c\cong 1$ in which cations are ordered in three dimensions. However, this structure is unstable, and only the cation superlattice ordering along the c axis remains upon returning to ambient conditions.

Carbonate anion orientation, which is a key differentiator between calcite and balcite structures, is tightly linked to the cation coordination and sensitive to different ratios of barium and calcium. It is expected that the formation and (de) stabilization of both the $R\bar{3}c$ superlattice and $R\bar{3}m$ supercell structures are mediated by carbonate anion orientation on a sublattice for which the carbon remains essentially fixed. While the most prominent peaks that gradually emerge upon heating under pressure are predominantly associated with cation ordering (Fig. 1e), a set of peaks associated with carbonate order appeared abruptly around

500 °C above a dramatically increased background (Fig. 1f). These structures appear to relax back to the dolomite-like superlattice structure upon returning to ambient conditions, suggesting that short-range restructuring occurs on both cation and anion lattices in response to changing pressure. To understand the mechanisms behind these transformations, the local structure of both carbonates and cations were investigated by solid-state NMR and XANES/EXAFS spectroscopy.

Solid-state NMR

Short-range carbonate order in balcites with different barium content was compared to natural Ba_{0.5}Ca_{0.5}CO₃ polymorphs alstonite and barytocalcite using direct excitation (DE) magic angle spinning (MAS) ¹³C NMR to determine whether the cation composition affects the carbonate environments. Peak position and width (isotropic chemical shift, $\delta_{\rm iso}$ ($\delta \nu$), in ppm) were used to determine the uniqueness and degree of disorder, respectively, of each carbonate environment. The barium content of balcite was shown by the ¹³C DE-MAS NMR spectra to have a negligible effect on carbonates in the as-synthesized material, yet a significant impact on its structure after heating (Fig. 2a and b).

Balcites precipitated from aqueous solutions with barium fractions of $x_{\text{feed}} = 0.24, 0.31, 0.41, 0.51$ exhibited one major peak centered at 167.6 ppm with a peak-

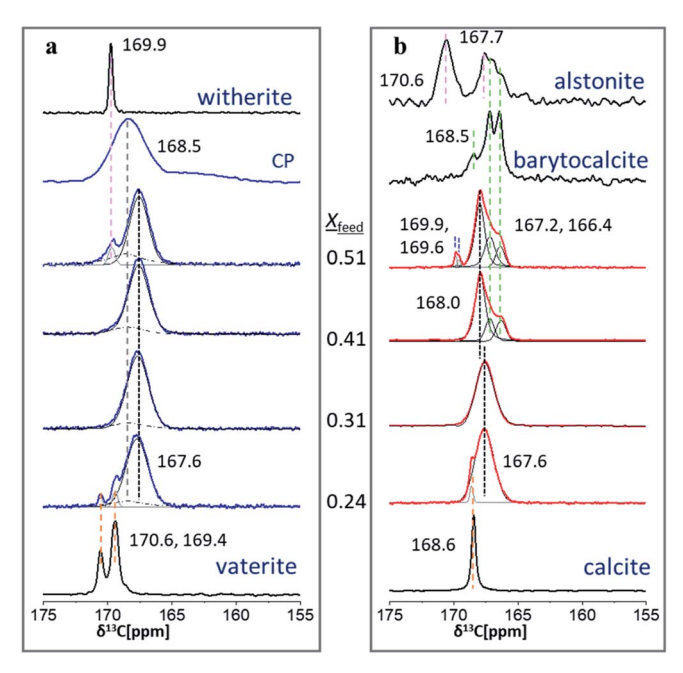


Fig. 2 13 C DE MAS NMR spectra of balcite, barytocalcite, and alstonite; the spectra of vaterite, calcite and witherite are added for comparison. (a) As-synthesized (blue) balcite samples with $x_{\rm feed}$ 0.24–0.51 and (b) after heating to 600 °C and cooling back to room temperature (red). A representative 13 C CP MAS spectrum of the balcite samples ((a) second from top, $x_{\rm feed} = 0.41$; denoted CP) demonstrates the occurrence of disordered hydrated carbonates in all balcite samples. Vertical dashed lines are provided to guide the eye to the different isotropic chemical shifts.

width of 2.0 ppm, ten-fold broader than that of calcite (168.6; <0.2 ppm) and witherite (169.9; <0.3 ppm).²³ The same chemical shifts and large peak widths across the various balcite compositions are indicative of disordered carbonate environments that do not depend on the barium content. Additionally 13 C CP MAS spectra identify that as-synthesized balcite contains disordered, hydrated carbonates.²³ Cross polarization (CP) NMR from hydrogen to carbon atoms is a complementary technique that selectively enhances the peaks of carbonate species in the vicinity of hydrogen. A notable hydrated carbonate peak (168.5; 3.0 ppm) in the CP MAS spectra (Fig. 2a; CP) of as-synthesized balcite is also present in DE MAS spectra (Fig. 2a; rectangle) and shows a hydrated carbonate content of \sim 15% in the three lower x balcites, and \sim 25% in the higher x balcite.

Balcite was annealed to 600 °C at 10 °C minute⁻¹ and cooled back to 25 °C at the same rate and re-examined by DE-MAS NMR (Fig. 2b). The balcite peak at 167.6 (1.6) ppm in x=0.24 and 0.31 samples did not change appreciably after heating, suggesting that short-range carbonate heterogeneity is retained. Vaterite present in the x=0.24 balcite sample (Fig. 2a) transformed to calcite upon heating (Fig. 2b), as evidenced by the replacement of the two vaterite peaks at 169.4 and 170.6 ppm with a single narrow calcite peak at 168.6 ppm. Absence of the peaks in the CP MAS spectra of heated balcites confirmed that heating dehydrated all carbonates, indicating that the disordered carbonate environments in the annealed materials are due to intrinsic structural disorder and not to defects induced by residual water molecules.

Upon annealing the x=0.41 and 0.51 balcite samples the balcite peak splits into at least three distinct components at 168.0, 167.2, and 166.4 ppm, each with \sim 1.0 ppm linewidth. Higher barium content resulted in higher intensity for the 167.2 ppm peak, changing the intensity ratio from approximately 4:1:1 at x=0.41 to 4:2:1 at x=0.51. Thus, three unique carbonate sites are established upon heating, of which at least one changes with differing amounts of calcium and barium. Witherite remained in the annealed x=0.51 sample as a secondary phase.

Alstonite and barytocalcite also contain multiple carbonate environments (Fig. 2b; top), some of which coincide with the chemical shift of those identified in annealed balcite. However, the presence of unique peaks and varying ratios between the peaks distinguished the three phases. Barytocalcite exhibits three peaks, 168.5 (0.7), 167.2 (1.3) and 166.4 (0.5) ppm. At least two are found at the same chemical shift as in annealed balcite, and have an intensity ratio similar to balcite with x = 0.51 (and same linewidths of 1.0 ppm). A third peak at 168.5 ppm is far lower in intensity relative to the other two peaks. Alstonite exhibited four peaks with an intensity ratio of approximately 8:6:1:1. A broad, intense peak at 170.6 (1.2) ppm clearly distinguishes it from all other structures examined. However, alstonite also had three peaks at 167.7 (0.5), 167.1 (1.3) and 166.2 (0.5) ppm that appear consistent with those in balcite and barytocalcite.

Mineral samples with natural ¹³C abundance had much lower signal-to-noise compared to isotopically enriched synthetic samples. Nonetheless, in all cases, multiple carbonate environments were present, at least one of which (167.2 ppm) appears to be present in each and is sensitive to the barium content. X-ray absorption spectroscopy at both the calcium and barium K-edge was used to obtain a complementary picture of the local structure and better understand the carbonate chemical shift sensitivity from the perspective of the cations.

XANES/EXAFS

Cation coordination numbers (CN) and symmetry of carbonate oxygens in the first coordination shell of the cations are reflected in the near-edge structure (XANES, Fig. 3a and d), while bond lengths and distances were extracted from fits to EXAFS data (Fig. 3b, c, e, f and Table 1) for calcite, witherite, and balcite with x = 0.5 and the ACBC from which it formed.

The position of the calcium K-edge edge (defined here as the maximum in the first derivative of the intensity) is very sensitive to the coordination number (CN), with a shift of 0.7 ± 0.1 eV towards higher energy (relative to the calcite edge) for each additional oxygen beyond the sixth.²⁴ The edge energy of ACBC and balcite were both shifted 0.5 eV relative to calcite, an indication that the average CN in both materials was between six and seven. A weak pre-edge feature corresponds to the $1s\to3d$ transition, ≈10 eV below the edge. This feature is a singlet and is markedly more intense in ACBC, indicating that the configuration of the first shell lacks an inversion center and is more disordered than calcite or barytocalcite.²⁵

Data in the calcium K-edge EXAFS region were fit in R-space with a structural model based on calcite (Fig. 3b, c and Table 1). Two separate distances were needed for each Ca–O₁ (first shell), Ca–C₁ (second shell), and Ca–O₂ (third shell) for both ACBC and balcite. ACBC had shorter Ca–O₁ distances (2.19, 2.39 Å) than balcite (2.37, 2.55 Å). The CN-weighted average Ca–O distance was 2.32 Å in ACBC compared to 2.42 Å in balcite, indicating that first-shell oxygen was more tightly

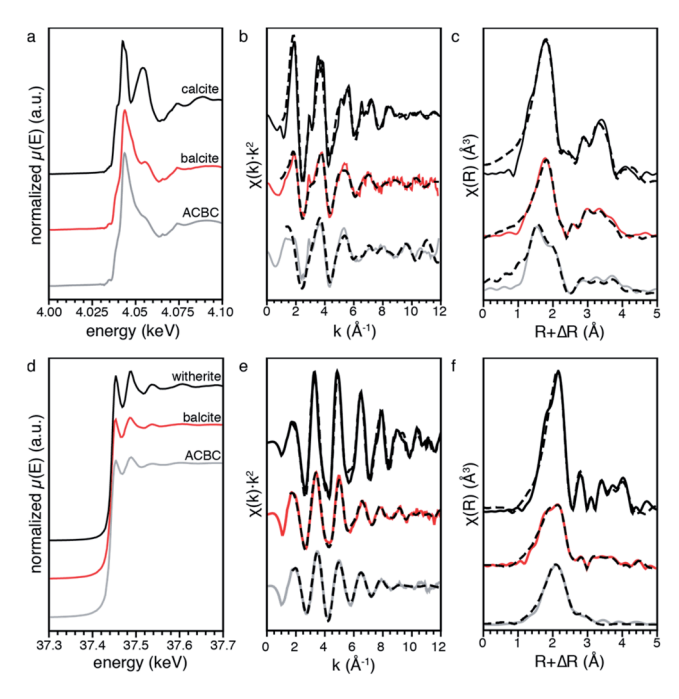


Fig. 3 X-ray absorption spectroscopy at the calcium K-edge (a–c) and barium K-edge (d–f) of calcite, balcite with x = 0.5, and ACBC with x = 0.55. (a and d) XANES, (b and e) k-space EXAFS, and (c and f) R-space EXAFS.

Table 1 XAS fitting parameters

	Ca K-edge			Ba K-edge		
	CN	R Ca-O (Å)	$\sigma^2 (\mathring{\text{A}}^2)$	CN	<i>R</i> Ba-O (Å)	$\sigma^2 (\mathring{\text{A}}^2)$
Calcite	6	2.39 (0.01)	0.010 (0.001)	_	_	_
ACBC	2.28,	2.19, 2.39	0.001, 0.004	3.17,	2.68, 2.83 (0.01)	0.005, 0.007 (0.002)
	4.22	(0.01)	(0.001)	4.83	, , ,	, , ,
Balcite	4.27,	2.37, 2.55	0.007, 0.006	1.74,	2.55, 2.73 (0.01)	0.006, 0.007 (0.001)
	2.23	(0.02)	(0.004)	6.26	, í	, ,
Witherite	e —	-	<u>-</u>	3, 4, 2	2.73, 2.85, 2.91 (0.02)	0.004, 0.008, 0.008 (0.004)

bound in the amorphous structure. The Debye–Waller factor, σ^2 , was appreciably higher in balcite (0.007, 0.006 Å²) than ACBC (0.001, 0.004 Å²). In addition, balcite required the inclusion of Ca–Ba (fourth shell) for the fit to converge.

Barium K-edge spectra of ACBC and balcite were qualitatively very similar, and differed only slightly from witherite (Fig. 3d). The edge energies of ACBC and balcite were both shifted -3.7 eV relative to witherite, an indication that the CN in these two materials was similar and less than nine. However, no correlation between oxygen CN and edge energy shift has been determined at the barium K-edge to our knowledge. In the EXAFS region, data were fit in k-space with a model based on witherite, but with a variable coordination number to account for the shift in edge energy in XANES. The CN of barium is eight in both ACBC and balcite, with CN weighted oxygen distances of 2.77 Å and 2.69 Å. This trend is opposite that of calcium, suggesting that crystallization of ACBC to balcite redistributes oxygen from barium to calcium while maintaining the same overall CN. Thus, transformation between ACBC and balcite leads to long-range crystalline order through subtle changes in short-range interactions.

Natural Ba_{0.5}Ca_{0.5}CO₃ polymorphs

To determine whether balcite could be synthesized from naturally occurring minerals by heating, alstonite from Alston mine, Cumberland, England was annealed under the same heating schedule as balcite (600 °C at a rate of 10 °C minute⁻¹ and held for 10 minutes, and cooling to 25 °C at the same rate, Fig. 4).

Alstonite undergoes a transformation to a structure resembling paralstonite starting at \sim 150 °C (Fig. 4). Paralstonite then converts back to alstonite (with larger lattice parameters due to the elevated temperature) starting around 530 °C. Upon holding this re-crystallized alstonite at 600 °C for 30 minutes, a transient conversion to another unknown intermediate is observed, which then rapidly converts to a balcite/balcomite-like structure.

Discussion

Heating balcite did not produce $Ba_{0.5}Ca_{0.5}CO_3$ polymorphs alstonite, paralstonite, or barytocalcite. Alstonite and paralstonite have similar aqueous solubilities to barytocalcite²⁶ and similar calculated cohesive energies,¹⁴ suggesting that they too should be more stable than balcite, which is unstable and nearly ~ 20 kJ mol⁻¹

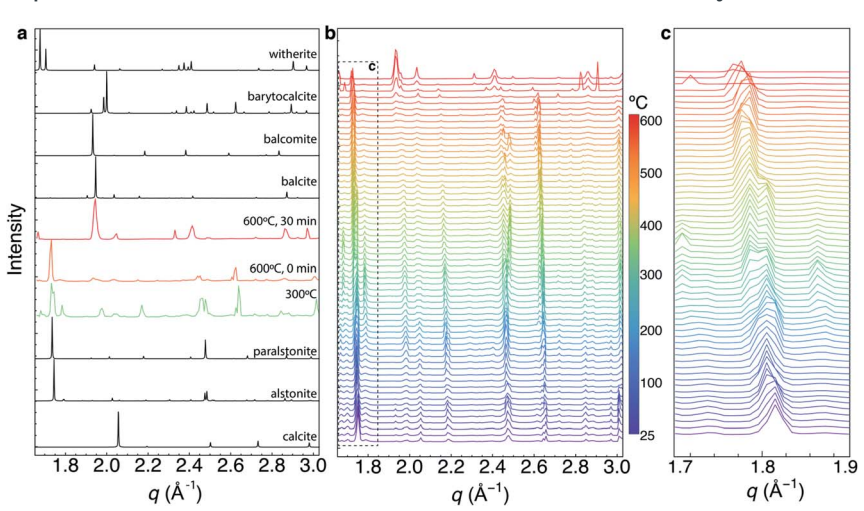


Fig. 4 (a) In situ WAXS of alstonite and paralstonite compared to XRD reference patterns for balcite, barytocalcite, calcite and witherite. (b) Alstonite transforms to paralstonite at $600~^{\circ}\text{C}$ through a number of structural intermediates at lower temperatures.

above the energetic ground state. 12 The sequence of transformations alstonite \rightarrow paralstonite \rightarrow alstonite \rightarrow balcomite suggests that alstonite is metastable relative to paralstonite at room temperature, but becomes more stable as the temperature increases. Surprisingly, barytocalcite did not form despite its reported stability on phase diagrams. 1,2,27 Together, these observations suggest that relative stability is not the primary driving force for transformations among metastable phases in this system.

We observed the formation of balcomite (Fig. 5) through continuous transformation upon annealing balcite, and a similar balcomite-like structure upon heating alstonite. This confirms that balcomite is the stable phase of Ba_{0.5}Ca_{0.5}CO₃ at elevated temperatures, and that perhaps a supercell balcomite-like phase is more stable under pressure given that the *in situ* experiments were conducted in a hermetically sealed crucible that was likely subjected to elevated pressure. These experiments also establish that paralstonite and alstonite interconvert *via* continuous, second-order transformations. Together, these observations indicate that continuous transformations are facilitated by similar short range order, but that transitions between structures with dissimilar local symmetry (*i.e.*, alstonite and balcomite) occur through discontinuous first-order transitions. We discuss the supporting evidence for both cation and anion ordering in the superlattice and supercell structures, culminating in a hypothetical structure for metastable end-member balcomite.

Cation ordering

Disordered cation distributions in as-synthesized balcite, ^{18,19} which originate from the ACBC precursor, ^{12,18} evolve towards superlattice and supercell ordering during heating. The observation of coarsening crystallites indicates that the ionic mobility is sufficient to undergo displacive transformation, but the structure nonetheless evolves continually. Specifically, cation ordering was observed in hr-

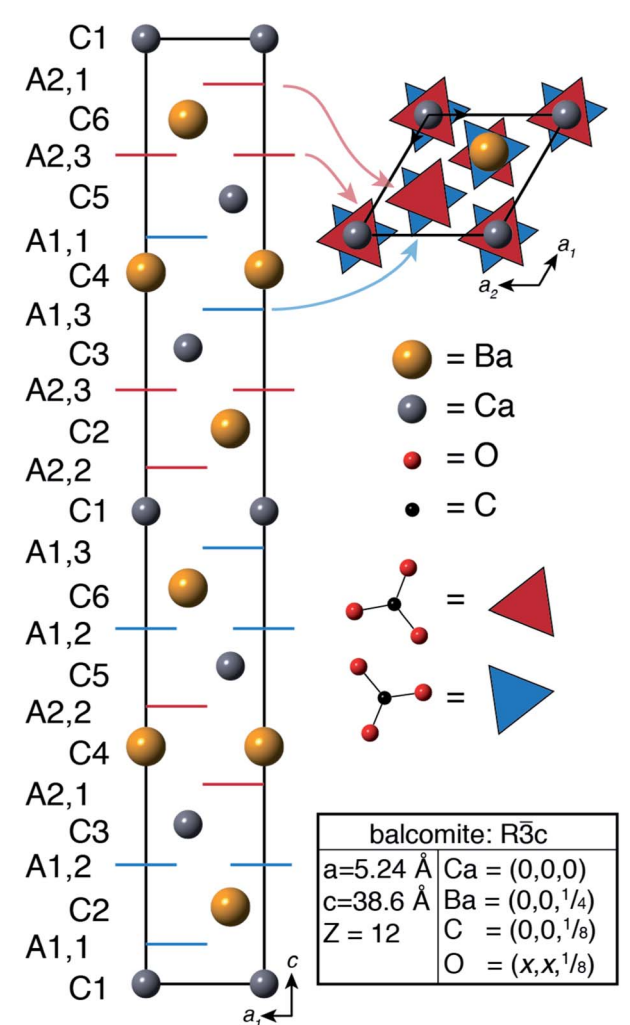


Fig. 5 Proposed structure of balcomite, towards which balcite transformed (but did not fully convert), at elevated temperature.

pXRD and *in situ* WAXS as the emergence of superlattice reflections (Fig. 1b and c). This is very similar to cation superlattice ordering of calcium and magnesium in dolomite^{21,28} (Ca_{0.5}Mg_{0.5}CO₃, spacegroup $R\bar{3}$) and barium and magnesium in norsethite²⁹ (Ba_{0.5}Mg_{0.5}CO₃ spacegroup $R\bar{3}m$).

Despite the symmetrical similarities between dolomite, norsethite, and balcomite, there are important differences, both structurally and energetically, between these phases. While dolomite and norsethite impart stability with respect to phase-separation,^{30,31} balcite is unstable under ambient conditions.¹² And while both dolomite and norsethite have calcite-like carbonate lattice sites that provide uniform 6-fold oxygen coordination number to each cation, annealed balcite exhibits at least three distinct carbonate environments (Fig. 3 and Table 1) with coordination numbers that differ between calcium (6–7) and barium (8–9).

Carbonate ordering

Cation ordering was accompanied by carbonate reorganization (Fig. 1d-f). Carbonates in as-synthesized balcite are highly disordered and are largely indistinguishable from those in ACBC (Fig. 2a and b). The cation CN does not change appreciably between ACBC and balcite, and the carbonates are only subtly redistributed such that they are slightly more closely bound to barium and slightly less so for calcium (Fig. 3 and Table 1). The balcite ¹³C NMR peak is five to ten times broader than that of calcite and witherite and more closely resembles mixed-cation lattices such as magnesian calcites. ³² Surprisingly, neither the peak position nor linewidth is affected by the barium content. The redistribution of this peak intensity into three distinct carbonate environments after heating confirms that the structural transformation observed in hr-pXRD is partially a result of carbonate reordering that occurs alongside cation segregation.

Carbonate rotational disorder at high temperatures is common. Calcite $(R\bar{3}c)$ undergoes a second-order phase transition to 'carbonate disordered' calcite IV approaching a critical temperature of $T_c = 970~^{\circ}\text{C.}^{33,34}$ This transition is characterized by the rotation of carbonates by 60° about their threefold axes, effectively inverting about the carbon center. Above $970~^{\circ}\text{C}$ calcite IV becomes further disordered into a 'carbonate-melted' calcite V with $R\bar{3}m$ symmetry.³⁵ The 'anomalous' increase in the stability of calcite relative to aragonite at higher temperatures arises from this carbonate rotational disorder due to the accompanying increase in configurational entropy.³⁶ Of particular relevance to this work, the temperature at which this transition occurs is dramatically reduced as the substitution of barium for calcium increases.³⁷

There are no reports in the Inorganic Crystal Structure Database of barium with less than 8-fold coordination, and low barium coordination numbers in the (6-fold coordinated) calcite lattice have been shown to be highly unfavorable.^{38,39} Witherite (BaCO₃ spacegroup *Pmcn*) undergoes a first-order transition to a calcite-type phase with *R3m* symmetry at 811 °C,⁴⁰ both with 9-fold coordination. This *R3m* phase has the same cation sublattice as calcite, but the apices of the carbonates are rotated 30° relative to those in the calcite lattice, and point the same direction in all carbonate planes. This allows one plane of carbonates to participate in bidentate coordination to the cation, while the other is in monodentate coordination, increasing the cation coordination number through a subtle change in anion orientation.

Balcomite structure

Based on evidence from hr-pXRD and *in situ* MAXS/WAXS, supported by NMR and XANES/EXAFS of precursor and reference materials, and using analogous carbonate systems to infer expected behavior of carbonate-cation local order, the balcomite structure is best understood as alternating cation and anion planes stacked along the *c*-axis in a calcite or dolomite-like unit cell.

Cations and anions each exhibit a different stacking sequence in the balcomite structure. Balcomite has dolomite-like cation ordering in which calcium-rich and barium-rich planes alternate along the *c*-axis. There are three unique cation planes in the balcite structure (C1, C2, and C3), but the introduction of superlattice ordering in balcomite doubles that number (*i.e.*, C4, C5, C6). The carbonate anions also lie on three unique planes (A1, A2, A3), but they can be oriented in one

of two ways in each lattice site (1 or 2), giving a total of six different anion planes

(A1,1; A1,2; A1,3; A2,1; A2,2; A2,3). Unlike other related carbonate structures, the orientation of carbonates follows a double-repeating pattern, whereby two A1 planes are followed by two A2 planes in order to simultaneously satisfy the preferred coordination number of both calcium (6) and barium (9).

Although the complete transformation to pure balcomite was not observed, the balcomite appears to be a metastable end-member structure towards which both balcite and alstonite transform. The result is an exotic superlattice structure with $R\bar{3}c$ symmetry in which 9-fold coordination around barium sites and 6-fold coordination around calcium sites can be achieved through continuous transformation from $R\bar{3}m$ balcite.

Implications for mineralogy

Second-order transitions were observed between both balcite and balcomite, and alstonite and paralstonite. Both systems appear to interconvert through some combination of local cation segregation and carbonate reorientation. These observations highlight the importance of local order on the pathways by which minerals interconvert. Metastable minerals, such as alstonite and paralstonite, may exist only under conditions in which the appropriate precursor was also favored. In the case of balcite and balcomite, these conditions are associated with the crystallite size of the intermediate phase. A reduction in the system energy through coarsening may reduce the driving force for the transformation to a more stable phase, but it appears that the more important consideration is whether any compositional changes that occur during coarsening give rise to increasing structural similarity. In addition, requirement to nucleate distinct local order may increase the kinetic barrier to transformation, allowing metastable polymorphs to persist for extended periods.

Experimental

Consumables

Unless otherwise noted, all aqueous solutions were prepared using ultra-pure water ($ho=18.2~ ext{M}\Omega$ cm) prepared with a Barnstead NanoDiamond UF + UV purification unit. Reagent grade (>99%) BaCl₂·2H₂O, CaCl₂·2H₂O, Na₂CO₃·2H₂O, CaCO₃, BaCO₃, (Sigma-Aldrich), were used without further purification. Iceland spar calcite was obtained from Dave's Down to Earth Rock Shop in Evanston, IL, USA. Witherite (cat #M21424), barytocalcite, alstonite, and paralstonite reference material was provided by the Field Museum of Natural History in Chicago, IL USA.

ACBC/balcite synthesis

Amorphous calcium barium carbonate (ACBC) was synthesized by rapid mixing of a cold aqueous solution of the alkaline earth chlorides ($[Ca^{2+}] + [Ba^{2+}] = 1$ M, pH 5.6-5.7, solution A) with a cold aqueous solution of Na₂CO₃ (1 M, pH 11.7, solution B). The mole fraction of Ba x_{feed} was varied between 0 and 1. For instance, to prepare solution A with $x_{\text{feed}} = 0.50$, 3.053 g BaCl₂·2H₂O (125 mmol) and 1.838 g CaCl₂·2H₂O (125 mmol) were dissolved in water to a final volume of 25 mL. For solution B, 3.100 g Na₂CO₃ (250 mmol) was dissolved in water to a final volume of 25 mL. Both solutions were then stored on ice for 2 h. Ice cold solution

B was rapidly added to solution A, mixed rapidly and thoroughly by vigorous shaking for 30 s.

To isolate ACBC, the resulting white precipitate was immediately collected by vacuum filtration through a 100 mm diameter Whatman no. 4 cellulose filter paper, washed 3 times with 5 mL cool water ($T=10\,^{\circ}\mathrm{C}$), and dried under vacuum (R.T., $p\approx 10\,\mathrm{Pa}=10^{-1}$ Torr, 24 h). ACBC crystallized within 24 hours when kept in its mother liquor at ambient conditions. Balcite was then collected by vacuum filtration using the same procedure as for ACBC, with an additional drying step at 110 °C for 1 hour.

Samples for NMR were prepared through the same procedure, but with 20% of the Na_2CO_3 enriched with ^{13}C to enhance the NMR sensitivity. Solutions with nominal $x_{\rm feed}=0.05,\ 0.10,\ 0.15,\ 0.30,\ 0.40,\ 0.50$ and 0.60 were used for NMR experiments.

High resolution synchrotron powder diffraction and Rietveld refinement

High resolution powder X-ray diffraction was acquired at sector 11-ID of the Advanced Photon Source at Argonne National Lab. A wavelength of $\lambda=0.414529$ Å (29.9097 keV) was set with a Si(111) double crystal (bounce-up geometry) and focused with a sagittally bent Si(111) crystal in the horizontal and a 1 meter Si/Pt mirror in the vertical, enabling a resolution of $2\theta=0.001^\circ$. Rietveld refinement was performed with GSAS using the EXPGUI graphical user interface.⁴¹ The scattering vector, Q, is defined as $Q=4\pi$ sin θ/λ with $Q=2\pi/d$ where d is the real-space distance between scatterers.

In situ synchrotron wide angle X-ray scattering

Low mass aluminum pans (TZero) were filled with approximately 20 mg of powder and hermetically sealed by crimping an aluminum lid to the top of the pan. The pans were annealed from 25 °C to 600 °C and cooled back to 25 °C at a rate of 10 °C min⁻¹ in a Linkam DSC600 temperature stage controlled with Linksys32 software. WAXS patterns were collected every minute at intervals of 10 °C. Diffuse rings consistent with a polycrystalline material were observed in two-dimensional CCD images. These images were radially integrated using GSAS-II.

Solid-state NMR

 1 H and 13 C NMR measurements were carried out on 500 and 300 MHz AVANCE III (Bruker) spectrometers using triple-resonance magic angle spinning (MAS) NMR probes with 4 mm zirconia rotors. Samples were spun at 5000 and 10 000 \pm 2 Hz. Direct 13 C excitation (DE) echo experiments were carried out with a 5.0 μs $\pi/2$, 10.0 μs π pulse widths, an echo interval τ equal to the rotor period T_R (200 and 100 μs), and TPPI 1 H decoupling at a level of 100 kHz. Relaxation delays of 1000 and 2400 s were employed to obtain fully relaxed spectra of the crystalline polymorphs, respectively. Cross polarization (CP) MAS echo experiments (indirect excitation) were carried out with a 5.0 μs $\pi/2$, 10.0 μs π pulse widths, an echo interval t (200 and 100 μs) identical to the rotor period T_R , a 1 H TPPI decoupling level of 100 kHz, Hartmann–Hahn RF levels were matched at 50 kHz, Hartmann–Hahn rf levels set at 50 kHz for 13 C, and ramped 1 H level (70–100 kHz), with contact times of 0.5, 1, and 2 ms and relaxation delays of 3 s for 13 C. Up to 16k transients were acquired. The chemical shifts of 13 C and 1 H are reported relative

to tetramethylsilane (TMS) and adamantane, respectively, with respective accuracies of ± 0.05 and ± 0.1 ppm; linewidths (δv ; full width at half maximum, FWHM) were determined with ± 0.1 ppm accuracy. Peak areas were calculated by deconvolution using DMFIT⁴² and Topspin.

X-ray absorption spectroscopy

ACBC (x=0.50) was synthesized as described above, and approximately half was left in the mother liquor to crystallize to balcite. Measurements were performed at the Dow–Northwestern–Dupont collaborative access team (DND-CAT), Sector 5-BM-D of the Advanced Photon Source at Argonne National Laboratory. Samples for Ca K-edge measurements were spread on 8 μ m Kapton tape and kept dry under a stream of He gas. For measurements performed at the Ba K-edge, powders were loaded into 1 mm OD quartz capillaries with 100 μ m thickness (Charles Supper). Calibration at the Ca K-edge was performed with a geological Iceland spar (calcite) standard, for which the edge energy was set at 4038 eV. ACBC samples were measured relative to this value. Molybdenum foil (Mo K-edge at 20.000 eV) was used to calibrate the Ba K-edge to an absolute scale.

Both the X-ray absorption near edge spectra (XANES) and extended X-ray absorption fine structure (EXAFS) spectra were analyzed using the Demeter package. 43 Normalization and background subtraction were carried out in Athena using Autobk. χ -Data were weighted by k, k^2 , and k^3 between 1.6 < k < 11.5 \mathring{A}^{-1} for the Ca K-edge and between $2 \le k \le 14 \text{ Å}^{-1}$ for the Ba K-edge. Fitting of the data to the crystal structures was performed using Artemis. The theoretical photoelectron scattering amplitudes and phase shifts were calculated using FEFF1. To generate the feff.inp file, which contains a list of the atomic coordinates centered at the absorbing atom, Atoms44 was used to calculate the atomic coordinates centered at Ca. The total theoretical $\chi(k)$ for each model was then constructed from the most important scattering paths and fit in R-space (Ca K-edge) or k-space (Ba K-edge). Multiple scattering was not considered. The coordination number, bond distance, Debye–Waller factor, amplitude reduction factor, S_0^2 , and shift in energy origin, ΔE_o, were determined previously.⁴⁵ Coordination numbers and Debye-Waller factors are highly correlated and were fit separately, but in each case with all other parameters floating. The validity of the fits was determined by the Rfactor, which was minimized to ≤ 0.01 .

Data in the calcium K-edge EXAFS region were fit in R-space with a structural model based on calcite (Fig. 3b, c and Table 1). Two separate distances were needed for each Ca–O₁ (first shell), Ca–C₁ (second shell), and Ca–O₂ (third shell) for both ACBC and balcite. ACBC had shorter Ca–O₁ distances (2.19, 2.39 Å) than balcite (2.37, 2.55 Å). The CN-weighted average Ca–O distance was 2.32 Å in ACBC compared to 2.42 Å in balcite, indicating that first-shell oxygen was more tightly bound in the amorphous structure. The Debye-Waller factors, σ^2 , were appreciably higher in balcite (0.007, 0.006 Å²) than ACBC (0.001, 0.004 Å²). In addition, balcite required the inclusion of Ca–Ba (fourth shell) for the fit to converge.

Five separate Ba–O distances in the witherite reference material were reduced to three to limit the number of free parameters given the resolution of the measurements (\sim 0.02 Å). Two separate oxygen distances and a CN of eight produced the best fit for both ACBC and balcite. Ba–O distances were longer in ACBC (2.68, 2.83) than balcite (2.55, 2.73 Å), with the CN-weighted averages of 2.77

Å and 2.69 Å, respectively. Only a single $Ba-C_1$ (second shell) was needed for a convergent fit to ACBC, while balcite required two $Ba-C_1$ distances, two $Ba-O_2$ (third shell) distances, Ba-Ca (fourth shell), and a $Ba-O_3$ (fifth shell).

Author contributions

All authors have given approval to the final version of the manuscript.

Conflicts of interest

There are no conflicts of interest.

Acknowledgements

AS and EP acknowledge the Israel Science Foundation grant 2001/17 for their financial support. AS and EP acknowledge the valuable assistance of Dr Shifi Kababya (Schulich Faculty of Chemistry, Technion, Israel).

References

- 1 A. F. Shatskiy, K. D. Litasov and Y. N. Palyanov, Phase relations in carbonate systems at pressures and temperatures of lithospheric mantle: review of experimental data, *Russ. Geol. Geophys.*, 2015, **56**(1-2), 113-142.
- 2 L. L. Chang, Subsolidus phase relations in the systems BaCO₃-SrCO₃, SrCO₃-CaCO₃, BaCO₃-CaCO₃, *J. Geol.*, 1965, 73(2), 346–368.
- 3 M. Dietzel, N. Gussone and A. Eisenhauer, Co-precipitation of Sr^{2+} and Ba^{2+} with aragonite by membrane diffusion of CO_2 between 10 and 50 degrees C, *Chem. Geol.*, 2004, 203(1-2), 139–151.
- 4 A. J. Tesoriero and J. F. Pankow, Solid Solution Partitioning of Sr²⁺, Ba²⁺, and Cd²⁺ to calcite, *Geochim. Cosmochim. Acta*, 1996, **60**(6), 1053–1063.
- 5 V. Mavromatis, K. E. Goetschl, C. Grengg, F. Konrad, B. Purgstaller and M. Dietzel, Barium partitioning in calcite and aragonite as a function of growth rate, *Geochim. Cosmochim. Acta*, 2018, 237, 65–78.
- 6 S. D. Škapin and I. Sondi, Homogeneous Precipitation of Mixed Anhydrous Ca-Mg-Ba-Sr carbonates by Enzyme-Catalyzed Reaction, *Cryst. Growth Des.*, 2005, 5(5), 1933–1938.
- 7 I. Sondi and E. Matijević, Homogeneous Precipitation by Enzyme-Catalyzed Reactions. 2. Strontium and Barium Carbonates, *Chem. Mater.*, 2003, 15, 1322–1326.
- 8 K. Benzerara, F. Skouri-Panet, J. Li, C. Ferard, M. Gugger, T. Laurent, E. Couradeau, M. Ragon, J. Cosmidis, N. Menguy, I. Margaret-Oliver, R. Tavera, P. Lopez-Garcia and D. Moreira, Intracellular Ca-carbonate biomineralization is widespread in cyanobacteria, *Proc. Natl. Acad. Sci. U. S. A.*, 2014, 111(30), 10933–10938.
- 9 E. Couradeau, et al., An early-branching microbialite cyanobacterium forms intracellular carbonates, *Science*, 2012, 336(6080), 459–462.
- 10 M. Aykol, S. S. Dwaraknath, W. Sun and K. A. Persson, Thermodynamic limit for synthesis of metastable inorganic materials, *Sci. Adv.*, 2018, 4, eaaq0148.

- 11 M. L. Whittaker, W. Sun, K. DeRocher, J. Saivenkataraman, G. Ceder and D. Joester, Structural basis for metastability in amorphous barium calcium carbonate, *Adv. Funct. Mater.*, 2018, **28**, 1704202.
- 12 M. L. Whittaker, W. Sun, D. O. Duggins, G. Ceder and D. Joester, Dynamic Barriers to Crystallization of Calcium Barium Carbonates, *Cryst. Growth Des.*, 2021, 21(8), 4556-4563.
- 13 W. Sun, S. T. Dacek, S. P. Ong, G. Hautier, A. Jain, W. D. Richards, A. C. Gamst, K. A. Persson and G. Ceder, The thermodynamic scale of inorganic crystalline metastability, *Sci. Adv.*, 2016, 2, e1600225.
- 14 R. Chuliá-Jordán, D. Santamaria-Perez, J. Ruiz-Fuertes, A. Otero-de-la-Roza and C. Popescu, Crystal Structure of BaCa(CO₃)₂ Alstonite Carbonate and Its Phase Stability upon Compression, *ACS Earth Space Chem.*, 2021, 5(5), 1130–1139.
- 15 R. M. Hazen, D. Papineau, W. Bleeker, R. T. Downs, J. M. Ferry, T. J. McCoy, D. A. Sverjensky and H. Yang, Mineral evolution, *Am. Mineral.*, 2008, 93(11–12), 1693–1720.
- 16 D. Spahr, L. Bayarjargal, V. Vinograd, R. Luchitskaia, V. Milman and B. Winkler, A new BaCa(CO₃)₂ polymorph, *Acta Crystallogr.*, *Sect. B: Struct. Sci.*, *Cryst. Eng. Mater.*, 2019, 75(Pt 3), 291–300.
- 17 P. N. Gavryushkin, A. B. Belonoshko, N. Sagatov, D. Sagatova, E. Zhitova, M. G. Krzhizhanovskaya, A. Rečnik, E. V. Alexandrov, I. V. Medrish, Z. I. Popov and K. D. Litasov, Metastable structures of CaCO₃ and their role in transformation of calcite to aragonite and postaragonite, *Cryst. Growth Des.*, 2021, 21(1), 65–74.
- 18 M. L. Whittaker and D. Joester, ACBC to Balcite: Bioinspired Synthesis of a Highly Substituted High-Temperature Phase from an Amorphous Precursor, *Adv. Mater.*, 2017, **29**(26), 1606730.
- 19 E. Seknazi, D. Levy, I. Polishchuk, A. Katsman and B. Pokroy, Experimental and Theoretical Insights into the Bioinspired Formation of Disordered Ba-Calcite, *Adv. Funct. Mater.*, 2020, **30**, 1805028.
- 20 L. Bindi, A. C. Roberts and C. Biagioni, The crystal structure of alstonite, BaCa(CO₃)₂: an extraordinary example of 'hidden' complex twinning in large single crystals, *Mineral. Mag.*, 2020, **84**(5), 699–704.
- 21 R. J. Reeder, Constraints on Cation Order in Calcium-rich Sedimentary Dolomite, *Aquat. Geochem.*, 2000, **6**, 213–226.
- 22 V. A. Drits, D. K. McCarty, B. A. Sakharov and K. L. Milliken, New insight into structural and compositional variability in some ancient excess-Ca dolomite, *Can. Mineral.*, 2005, 43, 1255–1290.
- 23 S. Kababya, A. Gal, K. Kahil, S. Weiner, L. Addadi and A. Schmidt, Phosphate-water interplay tunes amorphous calcium carbonate metastability: spontaneous phase separation and crystallization vs stabilization viewed by solid state NMR, J. Am. Chem. Soc., 2015, 137(2), 990–998.
- 24 F. E. Sowrey, L. J. Skipper, D. M. Pickup, K. O. Drake, Z. Lin, M. E. Smith and R. J. Newport, Systematic empirical analysis of calcium-oxygen coordination environment by calcium K-edge XANES, *Phys. Chem. Chem. Phys.*, 2004, **6**(1), 188–192.
- 25 J. L. Fulton, *et al.*, Understanding the effects of concentration on the solvation structure of Ca²⁺ in aqueous solution. I: The perspective on local structure from EXAFS and XANES, *J. Phys. Chem. A*, 2003, **107**(23), 4688–4696.

- 26 R. M. Garrels, M. E. Thompson and R. Siever, Stability of some carbonates at 25C and one atmosphere total pressure, *Am. J. Sci.*, 1960, **258**, 402–418.
- 27 L. L. Chang, Subsolidus phase relations in the systems BaCO₃-SrCO₃, SrCO₃-CaCO₃ and BaCO₃-CaCO₃, *J. Geol.*, 1965, 73(2), 346–368.
- 28 R. J. Reeder and Y. Nakamura, The Nature of Ordering and Ordering Defects in Dolomite, *Phys. Chem. Miner.*, 1982, **8**, 29–35.
- 29 H. Effenberger and J. Zemann, Single crystal X-ray investigation of norsethite, BaMg(CO₃)₂: one more mineral with an aplanar carbonate group, *Z. Kristallogr. Cryst. Mater.*, 1985, **171**(3–4), 275–280.
- 30 C. Pimentel and C. M. Pina, The formation of the dolomite-analogue norsethite: Reaction pathway and cation ordering, *Geochim. Cosmochim. Acta*, 2014, **142**, 217–223.
- 31 A. V. Radha and A. Navrotsky, Thermodynamics of Carbonates, *Rev. Mineral. Geochem.*, 2013, 77(1), 73–121.
- 32 J. Wang and U. Becker, Structure and carbonate orientation of vaterite (CaCO₃), Am. Mineral., 2009, 94(2-3), 380-386.
- 33 N. Ishizawa, Calcite V: a hundred-year-old mystery has been solved, *Powder Diffr.*, 2014, **29**(S1), S19–S23.
- 34 N. Ishizawa, H. Setoguchi and K. Yanagisawa, Structural evolution of calcite at high temperatures: phase V unveiled, *Sci. Rep.*, 2013, 3, 2832.
- 35 M. Farhadi Khouzani, D. M. Chevrier, P. Güttlein, K. Hauser, P. Zhang, N. Hedin and D. Gebauer, Disordered amorphous calcium carbonate from direct precipitation, *CrystEngComm*, 2015, 17(26), 4842–4849.
- 36 M. T. Dove and B. M. Powell, Neutron Diffraction Study of the tricritical orientational order/disorder phase transition in calcite at 1260K, *Phys. Chem. Miner.*, 1989, **16**, 503–507.
- 37 J. J. Lander, Polymorphism and Anion Rotational Disorder in the Alkaline Earth Carbonates, *J. Chem. Phys.*, 1949, 17(10), 892–901.
- 38 J. M. Astilleros, C. M. Pina, L. Fernández-Díaz and A. Putnis, The effect of barium on calcite {1014} surfaces during growth, *Geochim. Cosmochim. Acta*, 2000, **64**(17), 2965–2972.
- 39 M. Menadakis, G. Maroulis and P. G. Koutsoukos, Incorporation of Mg^{2^+} , Sr^{2^+} , Ba^{2^+} and Zn^{2^+} into aragonite and comparison with calcite, *J. Math. Chem.*, 2009, 46(2), 484-491.
- 40 S. M. Antao and I. Hassan, BaCO₃: high-temperature crystal structures and the Pmcn -> R3m phase transition at 811 degrees C, *Phys. Chem. Miner.*, 2007, 34(8), 573–580.
- 41 B. H. Toby and R. B. Von Dreele, GSAS-II: the genesis of a modern open-source all purpose crystallography software package, *J. Appl. Crystallogr.*, 2013, **46**(2), 544–549.
- 42 D. Massiot, F. Fayon, M. Capron, I. King, S. L. Calvé, B. Alonso, J.-O. Durand, B. Bujoli, Z. Gan and G. Hoatson, Modelling one- and two-dimensional solid-state NMR spectra, *Magn. Reson. Chem.*, 2002, 40, 70–76.
- 43 B. Ravel and M. Newville, ATHENA, ARTEMIS, HEPHAESTUS: data analysis for X-ray absorption spectroscopy using IFEFFIT, *J. Synchrotron Radiat.*, 2005, 12(4), 537–541.
- 44 B. Ravel, ATOMS: crystallography for the X-ray absorption spectroscopist, *J. Synchrotron Radiat.*, 2001, **8**, 314–316.

45 M. L. Whittaker, W. Sun, K. A. DeRocher, S. Jayaraman, G. Ceder and D. Joester, Structural Basis for Metastability in Amorphous Calcium Barium Carbonate (ACBC), *Adv. Funct. Mater.*, 2018, 28(2), 1704202.